Hindawi
Advances in Civil Engineering
Volume 2020, Article ID 6261917, 16 pages
https://doi.org/10.1155/2020/6261917

Research Article

Prediction of the Required Supporting Pressure for a Shallow Tunnel in Layered Rock Strata Based on 2D and 3D Upper Bound Limit Analysis

Hong-tao Wang,[1,2] **Chi Liu**,[3] **Ping Liu**,[1,2] **Xin Zhang**,[1,2] **and Yong Yang**[4]

[1]*School of Civil Engineering, Shandong Jianzhu University, Jinan 250101, China*
[2]*Key Laboratory of Building Structural Retrofitting and Underground Space Engineering (Shandong Jianzhu University), Ministry of Education, Jinan 250101, China*
[3]*Jinan Rail Transit Group Co., Ltd., Jinan 250101, China*
[4]*Shandong Academy of Building Research, Jinan 250031, China*

Correspondence should be addressed to Hong-tao Wang; wanghongtao918@163.com and Ping Liu; liuping19940321@163.com

Received 10 November 2019; Revised 25 April 2020; Accepted 28 May 2020; Published 13 July 2020

Academic Editor: Alessandro Palmeri

Determination of the required supporting pressure is the premise of tunnel support design. Only when the support design meets the requirements can the tunnel be safe and stable during construction and operation. This paper focuses on a shallow tunnel in layered rock strata and proposes a method for predicting the required supporting pressure. In this method, the 2D and 3D failure mechanisms are constructed, respectively. The analytical solutions of the supporting pressure corresponding to the two cases are derived on the basis of upper bound theorem and Hoek–Brown failure criterion. Then, the proposed method is validated by comparing with the results of existing research studies. Furthermore, a shallow tunnel in two-layer rock strata is chosen to illustrate the difference between the two solutions. The comparison shows that the supporting pressure in the 2D case is greater than that in the 3D case in general and it tends to be conservative for tunnel design. Conversely, the 3D solution may help to reduce the support cost. Furthermore, the change laws of the supporting pressure and failure range corresponding to varying parameters are obtained. These results may practically provide theoretical references for tunnel support design in layered rock strata.

1. Introduction

Now, as problems including heavy ground traffic and shortage of land resources have become increasingly acute in cities, construction of tunnels or other underground works has become a mainstream trend of urban development in the world. According to the burial depth, tunnels fall into two categories: shallow tunnels and deep tunnels. As for shallow tunnels, due to thin overlying rock strata, tunnel excavation has a great effect on ground disturbance; subsidence failure of surrounding rock masses is obvious. Especially when the geological conditions of tunneling strata are poor or in adverse conditions such as underground water, fault fracture zone, soft sand layer, and additional ground load, stability control over surrounding rock masses becomes more difficult. Once the support is unreasonable, disasters such as collapse are liable to occur, thus bringing a huge impact on engineering construction and operation safety.

As a hotspot, the researchers have carried out numerous research studies on the failure mechanism of shallow tunnels. In general, the following three research approaches can be employed: numerical simulation, theoretical analysis, and experimental method. For example, Karakouzian et al. [1] and Karami et al. [2] utilized the finite element method to investigate the effects of overburden height and internal transient pressure on the hydraulic fracturing of a concrete-lined pressure tunnel. The upper bound method is a classical theoretical analysis method. It has gained great recognitions

and extensive applications. In this method, a kinematically admissible velocity field for tunnel failure is required to be built in advance, and the limit load can be solved on the basis of the energy balance principle. By doing so, the complex and tedious calculation can be simplified effectively. Then, a close-to-actual failure mechanism can be obtained. For example, Leca and Dormieux [3] proposed three failure mechanisms of the tunnel face based on the movement of rigid conical blocks and obtained three upper bound solutions of the face pressure for a shallow tunnel driven in a frictional material. Lee and Nam [4] incorporated the influence of seepage force into the upper bound limit analysis of the tunnel face stability. Yamamoto et al. [5] focused on the stability of a square tunnel in cohesive-frictional soils subjected to surcharge loading and proposed the upper bound solutions for the ultimate surcharge loading by applying numerical limit analysis techniques. Mollon et al. [6] proposed two new continuous velocity fields for both collapse and blowout of an air-pressurized tunnel face in a purely cohesive soil and obtained the expressions of the collapse pressure using the upper bound method. Huang and Song [7] investigated the undrained stability of a plane strain tunnel heading in cohesive soil based on a multi-rigid-block mechanism. Zhang et al. [8] investigated the 3D failure characteristics of shallow circular tunnel faces in cohesive-frictional soils. Han et al. [9] and Li et al. [10, 11] investigated the influence of nonhomogeneity and anisotropy of soil masses on the face stability of shallow tunnels. In the abovementioned works, the soils or rocks in the strata are all regarded as the traditional Mohr–Coulomb materials.

In view of the nonlinear characteristics of the strength envelops when the soils or rocks fail [12–15], the nonlinear failure criteria may be more suitable to describe the failure of the tunnel's surrounding rock masses. Fraldi and Guarracino [16, 17] initially introduced the nonlinear Hoek–Brown failure criterion to analyze the roof collapse mechanisms for deep tunnels based on upper bound theorem. Recently, they [18] proposed a general characterization of tunnels depth and analyzed the collapse characteristics of intermediate tunnels. Based on their method, Huang and Yang [19] and Zhang et al. [20] conducted upper bound limit analysis on the roof collapse of deep circular tunnels. Furthermore, Yang and Huang [21], Huang et al. [22], and Guan et al. [23] proposed the three-dimensional collapse mechanisms of deep cavities in homogeneous Hoek–Brown rock masses. Qin et al. [24] and Yang et al. [25, 26] incorporated the nonhomogeneity and stratification characteristics of soil masses or rock masses into two-dimensional collapse analysis of deep tunnels. Similarly, they [27–30] also incorporated this influence into the three-dimensional mechanisms of deep tunnels or cavities. In the field of shallow tunnel collapse, Yang and Huang [31] proposed the collapse mechanism for a shallow circular tunnel. Yang and Li [32] conducted the upper bound limit analysis on roof collapse for a shallow tunnel in two-layered rock strata. Wang et al. [33, 34] proposed two kinds of collapse mechanisms for a shallow tunnel by incorporating the effects of changing groundwater table and pore water pressure. Lyu and Zeng [35] investigated the collapse of shallow tunnels in inclined rock stratum.

It is worth noticing that all the abovementioned research studies mainly focused on the prediction of tunnel collapse scope and mode. Specifically, in these works, the objective function constructed on the basis of the internal energy dissipation rate and the work rates done by external forces is the total energy dissipation rate. Moreover, the investigation on the shallow tunnel is relatively less on the whole. It should be noted that, due to smaller thickness of upper covering rock masses, the shallow tunnel is difficult to form an effective bearing arch structure inside the roof surrounding rocks and to liberate the self-bearing function of rock masses. Thus the determination of the required supporting pressure is of great significance to ensure the stability of shallow tunnels. Huang et al. [36] and Jiang et al. [37] once constructed the objective function of the supporting pressure and derived the analytical expressions of the required supporting pressure, but the tunnel's surrounding rock masses were assumed to be homogeneous and the proposed mechanisms were only limited to 2D case. The required roof supporting pressure for a shallow tunnel in layered rock strata and in 3D failure case needs further investigation. Consequently, based on the preceding research works, a shallow tunnel with arbitrary cross section in layered rock strata is chosen for study in this paper, and the 2D and 3D failure cases are considered simultaneously. The required supporting pressure corresponding to the 2D and 3D failure mechanisms is determined on the basis of the upper bound theorem. The effect of the thickness of varying rock strata, rock strength parameters, the additional ground load, etc. on the supporting pressure and failure range are also analyzed. The research results may serve as theoretical guidance for tunnel support design and construction in layered rock strata.

2. 2D and 3D Roof Failure Mechanisms for a Shallow Tunnel in Layered Rock Strata

A tunnel is a long and narrow underground structure. Therefore, it can be regarded as a plane strain problem to analyze the stress and deformation of the tunnel's surrounding rock masses. However, in actual engineering (Figure 1), tunnel collapse usually involves a typical 3D failure problem; the roof failure range is limited along the length of the tunnel. In addition, the thickness of the overlying rock strata is small for shallow tunnels; the roof failure often extends to the Earth's surface; as a result, a collapse arch bearing structure cannot be formed inside the surrounding rock masses; this is also an important reason why stability control over shallow tunnels is difficult. According to the abovementioned features, we propose the 2D and 3D failure mechanisms for a shallow rectangular tunnel in layered rock strata, respectively, as shown in Figure 2.

Specifically, in Figure 2, the tunnel burial depth is H; the roof includes n layers of rock masses; the thickness of each layer is h_i ($i = 1, 2, \ldots n$). In Figure 2(a), we assume that roof failure occurs in the xoy plane; the corresponding failure curve $f_i(x)$ ($i = 1, 2, \ldots n$) consists of n segments: $f_1(x)$, $f_2(x)$, $\ldots$ $f_n(x)$ for layer 1, layer 2, ... layer n, respectively.

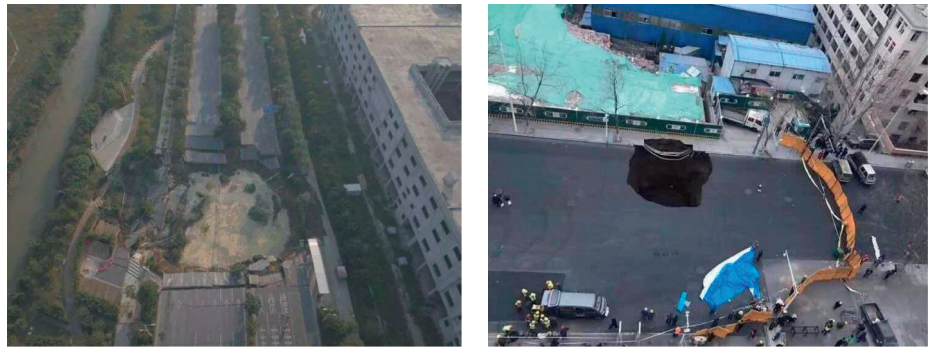

(a) (b)

Figure 1: Typical collapse accidents of China metro tunnels in 2018. (a) Foshan Metro Line 2 in Guangdong; (b) Tsingtao Metro Line 2.

Accordingly, in Figure 2(b), we assume that the rock masses within the failure range constitute a 3D axisymmetric rotating body, which may be formed by rotating the curve $f_i(x)$ in Figure 2(a) around the y axis within the xoy plane; the corresponding 3D failure surface equation for layer i is $f_i(x,z)$. Meanwhile, the roof failure is also affected by both the additional ground load σ_s and the supporting pressure q.

Furthermore, according to the existing indoor rock mechanics test results, in the $\sigma_n - \tau_n$ plane and the $\sigma_1 - \sigma_3$ plane, the strength envelope of the rock should be nonlinear rather than the linear relation used in the traditional Mohr–Coulomb strength criterion; a nonlinear strength criterion should be more suitable to describe the nonlinear failure characteristic of the tunnel's surrounding rock masses. Consequently, the widely used Hoek–Brown strength criterion [12, 13] is introduced in this paper. In the Mohr plane $\sigma_n - \tau_n$, it can be expressed as

$$\tau_n = A\sigma_c\left[(\sigma_n + \sigma_t)\sigma_c^{-1}\right]^B. \tag{1}$$

In equation (1), A and B are dimensionless empirical parameters related to properties of rock masses; τ_n and σ_n refer to the shear stress and normal stress at the rock fracture surface; and σ_c and σ_t refer to the compressive strength and tensile strength of the rock mass. Meanwhile, we assume that the roof rock masses are ideal rigid-plastic; failure of the rock masses meets the Hoek–Brown strength criterion and its associated flow rules. Accordingly, we may set the corresponding yield function F and the plastic potential function Q of rock failure to be equal; then, according to the potential theory, the plastic strain rates produced by rock failure in layer i may be solved by the following equation:

$$\dot{\varepsilon}_{ij} = \dot{\lambda}\frac{\partial Q}{\partial \sigma_{ij}} = \dot{\lambda}\frac{\partial F}{\partial \sigma_{ij}}, \tag{2}$$

where $\dot{\lambda}$ refers to the plasticity factor; $\dot{\varepsilon}_{ij}$ refers to the plasticity strain rate component; and and σ_{ij} refers to the stress component. The yield function F corresponding to the Hoek–Brown strength criterion can be expressed as follows:

$$F = \tau_n - A\sigma_c\left[(\sigma_n + \sigma_t)\sigma_c^{-1}\right]^B. \tag{3}$$

3. 2D Limit Analysis on the Required Supporting Pressure for a Shallow Tunnel

According to Chen's [38] theory, if the upper bound method is used to solve the required supporting pressure for a shallow tunnel, a kinematically admissible velocity field satisfying the deformation coordination needs to be established in advance; after the internal energy dissipation rate and external force power corresponding to the velocity field are obtained, the virtual work-rate equation can be constructed accordingly. Specifically, according to the failure mechanism shown in Figure 2(a), we may assume that the rock masses within the failure range are collapsing downward at the speed of v under the force of gravity and additional ground load. Conversely, the rock masses in the area that is not collapsing stay static. In addition, the rock masses are assumed to be ideal rigid-plastic. The collapsing rock masses and the surrounding static rock masses can be considered to be rigid, while the rock masses at the failure surfaces are in the plastic flow state. Consequently, internal energy dissipation occurs only at the roof failure surfaces.

Accordingly, the failure curve $f_i(x)$ in layer i is a velocity discontinuity line. We may obtain the plastic shear strain rate $\dot{\gamma}_{ni}$ and plastic normal strain rate $\dot{\varepsilon}_{ni}$ at the failure surface by substituting equation (3) into equation (2). Thus, the corresponding internal energy dissipation rate in layer i can be expressed as follows:

$$\begin{aligned}\dot{D}_i &= \sigma_{ni}\dot{\varepsilon}_{ni} + \tau_{ni}\dot{\gamma}_{ni} \\ &= \frac{\left[-\sigma_{ti} + \sigma_{ci}\left(A_iB_i\right)^{\left(1/\left(1-B_i\right)\right)}\left(1 - B_i^{-1}\right)f_i'(x)^{\left(1/\left(1-B_i\right)\right)}\right]}{\left[w_i\sqrt{1 + f_i'(x)^2}\right]},\end{aligned} \tag{4}$$

where w_i refers to the thickness of the failure surface in layer i.

Considering the symmetry of the 2D failure mechanism, half of the failure range is selected for study. By integrating equation (4) along the n failure surfaces in all rock layers, we obtain the equation for the total rate of internal energy dissipation:

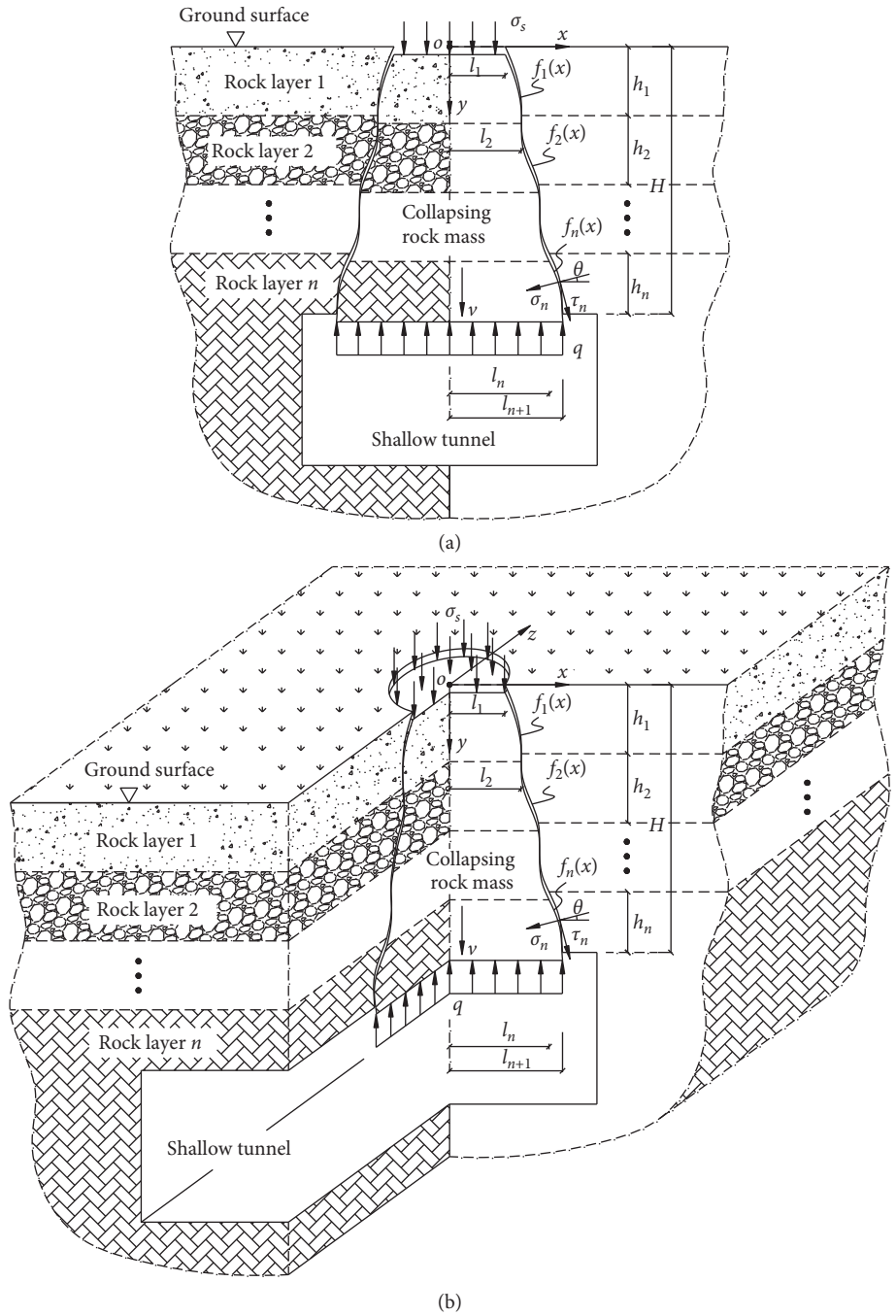

Figure 2: 2D and 3D failure mechanisms for a shallow tunnel in layered rock strata. (a) 2D failure mechanism; (b) 3D failure mechanism.

$$W_D = \sum_{i=1}^{n} \int_{l_i}^{l_{i+1}} \left[-\sigma_{ti} + \sigma_{ci} \left(A_i B_i\right)^{\left(1/\left(1-B_i\right)\right)} \cdot \left(1 - B_i^{-1}\right) f_i'(x)^{\left(1/\left(1-B_i\right)\right)} \right] \mathrm{d}x \cdot v, \tag{5}$$

where l_i ($i = 1, 2, \ldots, n$) refers to the half width of the failure range in layer i.

The work rate done by the weight of the collapsing rock masses is

$$W_\gamma = \left\{ \sum_{i=1}^{n} \gamma_i h_i l_i + \sum_{i=1}^{n} \int_{l_i}^{l_{i+1}} \gamma_i \left[\sum_{j=1}^{i} h_j - f_i(x) \right] dx \right\} v, \tag{6}$$

where γ_i is the unit weight of rock layer i.

The work rate produced by the additional ground load is

$$W_{\sigma_s} = \sigma_s l_1 v. \tag{7}$$

The work rate produced by the supporting pressure is

$$W_q = -q l_{n+1} v. \tag{8}$$

Based on equations (6)–(8), we can obtain the total work rate done by external forces. Then, by using the virtual work-rate principle, we obtain

$$-W_D = W_\gamma + W_q + W_{\sigma_s}. \tag{9}$$

Substituting equations (5)–(8) into equation (9) yields

$$\sum_{i=1}^{n}\int_{l_i}^{l_{i+1}}\left[\sigma_{ti} - \sigma_{ci}\left(A_iB_i\right)^{\left(1/\left(1-B_i\right)\right)}\left(1-B_i^{-1}\right)f_i'(x)^{\left(1/\left(1-B_i\right)\right)}\right]\mathrm{d}x = \sum_{i=1}^{n}\gamma_i h_i l_i + \sum_{i=1}^{n}\int_{l_i}^{l_{i+1}}\gamma_i\left[\sum_{j=1}^{i}h_j - f_i(x)\right]\mathrm{d}x - ql_{n+1} + \sigma_s l_1. \tag{10}$$

According to equation (10), the required roof supporting pressure for a shallow tunnel can be expressed as

$$q = l_{n+1}^{-1}\sum_{i=1}^{n}\int_{l_i}^{l_{i+1}}\Lambda_i\left[x, f_i(x), f_i'(x)\right]\mathrm{d}x + l_{n+1}^{-1}\sum_{i=1}^{n}\gamma_i h_i l_i + \sigma_s l_1 l_{n+1}^{-1}, \tag{11}$$

where $\Lambda_i[x, f_i(x), f_i'(x)]$ is

$$\Lambda_i\left[x, f_i(x), f_i'(x)\right] = -\sigma_{ti} + \sigma_{ci}\left(A_iB_i\right)^{\left(1/\left(1-B_i\right)\right)}\cdot\left(1-B_i^{-1}\right)f_i'(x)^{\left(1/\left(1-B_i\right)\right)} + \gamma_i\sum_{j=1}^{i}h_j - \gamma_i f_i(x). \tag{12}$$

Equation (11) is a functional of x and $f_i(x)$. According to the upper bound theorem, in all potential roof failure mechanisms, the $f_i(x)$ corresponding to the real mechanism shall enable equation (11) to obtain the maximum value. This is a typical variational problem. The following Euler–Lagrange equation can be used to obtain the optimal upper bound solution:

$$\frac{\partial\Lambda_i}{\partial f_i(x)} - \frac{\partial}{\partial x}\left(\frac{\partial\Lambda_i}{\partial f_i'(x)}\right) = 0. \tag{13}$$

Substituting equation (12) into equation (13) results in

$$-\gamma_i + \left(1-B_i\right)^{-1}\sigma_{ci}\left(A_iB_i\right)^{\left(1/\left(1-B_i\right)\right)} f_i'(x)^{\left(\left(2B_i-1\right)/\left(1-B_i\right)\right)} f_i''(x) = 0. \tag{14}$$

By integrating equation (14), we obtain

$$f_i'(x) = A_i^{-1/B_i}B_i^{-1}\left(\gamma_i x + C_i\right)^{\left(1-B_i\right)/B_i}\sigma_{ci}^{\left(B_i-1\right)/B_i}, \tag{15}$$

where C_i is the constant to be determined. According to the progressive failure characteristics of the roof's surrounding rock masses, the failure surface should be first formed in the bottom, continue to develop upward, and eventually extend to the Earth's surface. Similarly, in layer i, rock failure also develops upward from the bottom of this layer. In addition, the layer i is internally homogeneous. If the rock failure in layer i does not extend to the upper layer, this is very similar to the failure characteristics in homogeneous formation. Furthermore, according to the symmetry of the 2D failure mechanism in Figure 2(a) and the failure characteristics in homogeneous rock media [16, 17], the first derivative of $f_i(x)$ in layer i is set equal to 0 at the point $x = 0$; then parameter C_i can be determined as 0 and equation (15) can be expressed as

$$f_i'(x) = \xi_i B_i^{-1}x^{\left(\left(1-B_i\right)/B_i\right)}, \tag{16}$$

where $\xi_i = A_i^{\left(-1/B_i\right)}\gamma_i^{\left(\left(1-B_i\right)/B_i\right)}\sigma_{ci}^{\left(\left(B_i-1\right)/B_i\right)}$.

By integrating equation (16), we obtain

$$f_i(x) = \xi_i x^{\left(1/B_i\right)} + D_i. \tag{17}$$

Furthermore, by substituting equations (16) and (17) into equation (12), we obtain

$$\Lambda_i\left[x, f_i(x), f_i'(x)\right] = -\sigma_{ti} + \sigma_{ci}\left(A_iB_i\right)^{1/\left(1-B_i\right)}\cdot\left(1-B_i^{-1}\right)\xi_i^{1/\left(1-B_i\right)}B_i^{1/\left(1-B_i\right)}x^{1/B_i} + \gamma_i\sum_{j=1}^{i}h_j - \gamma_i\xi_i x^{1/B_i} - \gamma_i D_i. \tag{18}$$

Equation (18) is substituted into equation (11) to obtain the required roof supporting pressure:

$$q = l_{n+1}^{-1}\sum_{i=1}^{n}\left\{\left(-\sigma_{ti} + \gamma_i\sum_{j=1}^{i}h_j - \gamma_i D_i\right)\left(l_{i+1} - l_i\right) + B_i\left(1+B_i\right)^{-1}\left[\sigma_{ci}A_i^{\left(1/\left(1-B_i\right)\right)}\left(1-B_i^{-1}\right)\xi_i^{\left(1/\left(1-B_i\right)\right)} - \gamma_i\xi_i\right]\cdot\left(l_{i+1}^{\left(\left(1+B_i\right)/B_i\right)} - l_i^{\left(\left(1+B_i\right)/B_i\right)}\right)\right\} + l_{n+1}^{-1}\sum_{i=1}^{n}\gamma_i h_i l_i + \sigma_s l_1 l_{n+1}^{-1}. \tag{19}$$

Note that the required supporting pressure involved in equation (19) is a function related to the width l_i of the failure range and increases with the increase of l_i. To ensure the safety of engineering design, the worst case of roof failure shall be considered. Specifically, we may set the bottom width of the failure range to be equal to the tunnel width; in this case, the tunnel requires the maximum supporting pressure, which can be obtained by

$$q = l_t^{-1}\sum_{i=1}^{n}\left\{\left(-\sigma_{ti} + \gamma_i\sum_{j=1}^{i}h_j - \gamma_i D_i\right)\left(l_{i+1} - l_i\right) + B_i\left(1+B_i\right)^{-1}\left[\sigma_{ci}A_i^{1/\left(1-B_i\right)}\left(1-B_i^{-1}\right)\xi_i^{1/\left(1-B_i\right)} - \gamma_i\xi_i\right]\left(l_{i+1}^{\left(\left(1+B_i\right)/B_i\right)} - l_i^{\left(1+B_i\right)/B_i}\right)\right\} + l_t^{-1}\sum_{i=1}^{n}\gamma_i h_i l_i + \sigma_s l_1 l_t^{-1}, \tag{20}$$

where l_t (half width of the tunnel) shall meet $l_{i+1}|_{i=n} = l_t$. In equation (20), D_i and l_i ($i = 1, 2, 3, \ldots n$) are still unknown. According to the geometrical relationships in Figure 2(a), the failure curve $f_i(x)$ meets

$$\begin{cases} f_1(x)\big|_{x=l_1} = 0, \\ f_1(x)\big|_{x=l_2} = f_2(x)\big|_{x=l_2} = h_1, \\ f_2(x)\big|_{x=l_3} = f_3(x)\big|_{x=l_3} = h_1 + h_2, \\ \ldots, \\ f_{n-1}(x)\big|_{x=l_n} = f_n(x)\big|_{x=l_n} = h_1 + h_2 + \ldots + h_{n-1}, \\ f_n(x)\big|_{x=l_{n+1}} = H. \end{cases} \tag{21}$$

By substituting equation (17) into equation (21), we obtain the integration constant D_i:

$$\begin{cases} D_1 = -\xi_1 l_1^{(1/B_1)}, \\ D_2 = h_1 - \xi_2 l_2^{(1/B_2)}, \\ D_3 = h_1 + h_2 - \xi_3 l_3^{(1/B_3)}, \\ \ldots, \\ D_n = h_1 + h_2 + \ldots + h_{n-1} - \xi_n l_n^{(1/B_n)}. \end{cases} \tag{22}$$

Furthermore, the following equations can be derived from equation (21).

$$\begin{cases} \xi_1 l_2^{(1/B_1)} - \xi_1 l_1^{(1/B_1)} = h_1, \\ \xi_2 l_3^{(1/B_2)} - \xi_2 l_2^{(1/B_2)} = h_2, \\ \xi_3 l_4^{(1/B_3)} - \xi_3 l_3^{(1/B_3)} = h_3, \\ \ldots, \\ \xi_{n-1} l_n^{(1/(B_{n-1}))} - \xi_{n-1} l_{n-1}^{(1/(B_{n-1}))} = h_{n-1}, \\ \xi_n l_{n+1}^{(1/(B_n))} - \xi_n l_n^{(1/(B_n))} = h_n. \end{cases} \tag{23}$$

Based on equations (21)–(23), the width l_i and constant D_i can be solved. Then the required supporting pressure and the failure range for the shallow tunnel in the 2D failure case can be determined accordingly.

4. 3D Limit Analysis on the Required Supporting Pressure for a Shallow Tunnel

As shown in Figure 2(b), in the case of 3D roof failure for a shallow tunnel, the specific derivation process of the required supporting pressure is in accordance with that in Section 3. Similarly, the rotational collapsing rock masses are assumed to be a rigid block with the downward velocity of v. The failure surface in layer i is approximately conical. The plastic strain rates can also be solved by using equations (2) and (3). Consequently, by integrating equation (4) along the 3D failure surfaces, we obtain the equation for calculating the total rate of internal energy dissipation:

$$W_D = 2\pi \sum_{i=1}^{n} \int_{l_i}^{l_{i+1}} \left[-\sigma_{ti} x + \sigma_{ci} (A_i B_i)^{(1/(1-B_i))} \cdot \left(1 - B_i^{-1}\right) x f_i'(x)^{(1/(1-B_i))} \right] \mathrm{d}x \cdot v, \tag{24}$$

where l_i ($i = 1, 2, \ldots, n$) refers to the radius of the rotational failure block in layer i, and it is similar to the half width of the failure range in the 2D case.

The work rate done by the weight of collapsing rock masses is

$$W_\gamma = \left\{ \sum_{i=1}^{n} \pi \gamma_i h_i l_i^2 + 2\pi \sum_{i=1}^{n} \int_{l_i}^{l_{i+1}} \gamma_i \left[\sum_{j=1}^{i} h_j x - x f_i(x) \right] \mathrm{d}x \right\} v, \tag{25}$$

The work rate produced by the additional ground load is

$$W_{\sigma_s} = \pi \sigma_s l_1^2 v. \tag{26}$$

The work rate produced by the supporting pressure is

$$W_q = -\pi q l_{n+1}^2 v. \tag{27}$$

Based on equations (24)–(27), the virtual work-rate principle can be utilized to obtain the following equation:

$$2 \sum_{i=1}^{n} \int_{l_i}^{l_{i+1}} \left[\sigma_{ti} x - \sigma_{ci} (A_i B_i)^{(1/(1-B_i))} \left(1 - B_i^{-1}\right) x f_i'(x)^{(1/(1-B_i))} \right] \mathrm{d}x = \sum_{i=1}^{n} \gamma_i h_i l_i^2 + 2 \sum_{i=1}^{n} \int_{l_i}^{l_{i+1}} \gamma_i \left[\sum_{j=1}^{i} h_j x - x f_i(x) \right] \mathrm{d}x - q l_{n+1}^2 + \sigma_s l_1^2. \tag{28}$$

Then, the required supporting pressure in the 3D case can be solved as

$$q = 2 l_{n+1}^{-2} \sum_{i=1}^{n} \int_{l_i}^{l_{i+1}} \Lambda_i [x, f_i(x), f_i'(x)] \mathrm{d}x + l_{n+1}^{-2} \sum_{i=1}^{n} \gamma_i h_i l_i^2 + \sigma_s l_1^2 l_{n+1}^{-2}, \tag{29}$$

where $\Lambda_i [x, f_i(x), f_i'(x)]$ is

$$\Lambda_i [x, f_i(x), f_i'(x)] = -\sigma_{ti} x + \sigma_{ci} (A_i B_i)^{(1/(1-B_i))} \cdot \left(1 - B_i^{-1}\right) x f_i'(x)^{(1/(1-B_i))} + \gamma_i \sum_{j=1}^{i} h_j x - \gamma_i x f_i(x). \tag{30}$$

Similarly, to obtain the optimal upper bound solution, we can also use the Euler–Lagrange equation in equation (13). Thus, by substituting equation (30) into equation (13), we obtain

$$-\gamma_i x + \sigma_{ci} (A_i B_i)^{(1/(1-B_i))} B_i^{-1} f_i'(x)^{(B_i/(1-B_i))} + (1 - B_i)^{-1} \sigma_{ci} (A_i B_i)^{(1/(1-B_i))} x f_i' \cdot (x)^{((2B_i-1)/(1-B_i))} f_i''(x) = 0. \tag{31}$$

By integrating equation (31), we obtain

$$f_i'(x) = \left(\frac{1}{2}\gamma_i x + \frac{E_i}{x}\right)^{(1-B_i)/B_i} \sigma_{ci}^{(B_i-1)/B_i} A_i^{-1/B_i} B_i^{-1}, \tag{32}$$

where E_i is an unknown constant.

Note that it is very complicated and difficult to solve equation (32) to obtain the analytical expression of $f_i(x)$. To facilitate engineering design, the handling method of equation (15) in Section 3 can be utilized to solve this problem. Specifically, the failure characteristics in homogeneous strata and the symmetry of the 3D rotational failure surfaces shall be taken into consideration. The first derivative of $f_i(x)$ can also be assumed to be zero at the point $x = 0$; then the constant E_i here can be determined as zero. Furthermore, equation (32) can be expressed as

$$f_i'(x) = \eta_i B_i^{-1} x^{\left((1-B_i)/B_i\right)}, \tag{33}$$

where $\eta_i = (2\sigma_{ci}/\gamma_i)^{((B_i-1)/B_i)} A_i^{(-1/B_i)}$.

Furthermore, by integrating equation (33), we obtain

$$f_i(x) = \eta_i x^{(1/B_i)} + F_i, \tag{34}$$

where F_i is another unknown constant.

Based on equation (34), the equation of the 3D failure surface can be expressed as

$$y = f_i(x,z) = \eta_i\left(x^2 + z^2\right)^{(1/2B_i)} + F_i. \tag{35}$$

Substituting equations (33) and (34) into equation (30) results in

$$\begin{aligned}\Lambda_i[x, f_i(x), f_i'(x)] = {} & -\sigma_{ti}x + \sigma_{ci}(A_iB_i)^{1/(1-B_i)} \\ & \cdot \left(1 - B_i^{-1}\right)\eta_i^{1/(1-B_i)} B_i^{1/(1-B_i)} \\ & \cdot x^{(1+B_i)/B_i} + \gamma_i \sum_{j=1}^{i} h_j x - \gamma_i\eta_i x^{(1+B_i)/B_i} \\ & - \gamma_i F_i x.\end{aligned} \tag{36}$$

Furthermore, substituting equation (36) into equation (29) results in

$$\begin{aligned}q = {} & l_{n+1}^{-2} \sum_{i=1}^{n} \left\{ \left(-\sigma_{ti} + \gamma_i \sum_{j=1}^{i} h_j - \gamma_i F_i \right)\left(l_{i+1}^2 - l_i^2\right) \right. \\ & + 2B_i\left(1 + 2B_i\right)^{-1}\left[\sigma_{ci} A_i^{1/(1-B_i)}\left(1 - B_i^{-1}\right)\eta_i^{1/(1-B_i)}\right. \\ & \left.\left. - \gamma_i\eta_i\right]\left(l_{i+1}^{(1+2B_i)/B_i} - l_i^{(1+2B_i)/B_i}\right) \right\} \\ & + l_{n+1}^{-2} \sum_{i=1}^{n} \gamma_i h_i l_i^2 + \sigma_s l_1^2 l_{n+1}^{-2}.\end{aligned} \tag{37}$$

Similarly, to ensure the safety of engineering design, according to the design principle for the worst case in Section 3, we set the bottom width of the failure block to be equal to the tunnel width. Then the required supporting pressure corresponding to the 3D mechanism in Figure 2(b) can be expressed as

$$\begin{aligned}q = {} & l_t^{-2} \sum_{i=1}^{n} \left\{ \left(-\sigma_{ti} + \gamma_i \sum_{j=1}^{i} h_j - \gamma_i F_i \right)\left(l_{i+1}^2 - l_i^2\right) \right. \\ & + 2B_i\left(1 + 2B_i\right)^{-1}\left[\sigma_{ci} A_i^{(1/(1-B_i))}\left(1 - B_i^{-1}\right)\eta_i^{(1/(1-B_i))}\right. \\ & \left.\left. - \gamma_i\eta_i\right]\left(l_{i+1}^{((1+2B_i)/B_i)} - l_i^{((1+2B_i)/B_i)}\right) \right\} + l_t^{-2} \sum_{i=1}^{n} \gamma_i h_i l_i^2 + \sigma_s l_1^2 l_t^{-2}\end{aligned} \tag{38}$$

The unknown parameters can be solved by using the geometrical relationships in Figure 2(b). Particularly, the curve $f_i(x)$ $(i = 1, 2, 3, \ldots n)$ meets the following equations.

$$\begin{cases} f_1(x)\big|_{x=l_1} = 0, \\ f_1(x)\big|_{x=l_2} = f_2(x)\big|_{x=l_2} = h_1, \\ f_2(x)\big|_{x=l_3} = f_3(x)\big|_{x=l_3} = h_1 + h_2, \\ \ldots, \\ f_{n-1}(x)\big|_{x=l_n} = f_n(x)\big|_{x=l_n} = h_1 + h_2 + \ldots + h_{n-1}, \\ f_n(x)\big|_{x=l_{n+1}} = H. \end{cases} \tag{39}$$

By substituting equation (34) into equation (39), we obtain

$$\begin{cases} F_1 = -\eta_1 l_1^{(1/B_1)}, \\ F_2 = h_1 - \eta_2 l_2^{(1/B_2)}, \\ F_3 = h_1 + h_2 - \eta_3 l_3^{(1/B_3)}, \\ \ldots, \\ F_n = h_1 + h_2 + \ldots + h_{n-1} - \eta_n l_n^{(1/B_n)}. \end{cases} \tag{40}$$

Furthermore, the following equations can also be derived from equation (39):

$$\begin{cases} \eta_1 l_2^{(1/B_1)} - \eta_1 l_1^{(1/B_1)} = h_1, \\ \eta_2 l_3^{(1/B_2)} - \eta_2 l_2^{(1/B_2)} = h_2, \\ \eta_3 l_4^{(1/B_3)} - \eta_3 l_3^{(1/B_3)} = h_3, \\ \ldots, \\ \eta_{n-1} l_n^{(1/(B_{n-1}))} - \eta_{n-1} l_{n-1}^{(1/(B_{n-1}))} = h_{n-1}, \\ \eta_n l_{n+1}^{(1/(B_n))} - \eta_n l_n^{(1/(B_n))} = h_n. \end{cases} \tag{41}$$

By combining equations (39)–(41), we can determine the constant F_i and the radius l_i of the 3D failure block. Then the required supporting pressure and the failure range of the shallow tunnel in the 3D case can be determined.

5. Results and Discussion

5.1. Comparison with Existing Research Studies. In order to predict the required supporting pressure for shallow tunnels, Huang et al. [36] proposed the failure mechanism of a rectangular tunnel in homogeneous rock media and derived a 2D analytical solution of supporting pressure. Accordingly, in order to validate the effectiveness of the proposed method in this paper, we set the strength parameters of all rock layers in Figure 2(a) to be the same value; now this mechanism can be turned into the mechanism by Huang et al. [36]. Furthermore, Figure 3 lists the comparison results between the required supporting pressure calculated by this paper and that calculated by Huang et al. [36]. The comparison involves the following parameters: $l_t = 5\,m$ and $10\,m$, $A = 0.15$, $B = 0.85$, $\sigma_c = 0.5$ MPa, $\sigma_t = (\sigma_c/100)$, $\gamma = 18\,\text{kN}/m^3$, and $\sigma_s = 50$ kPa. It can be seen from Figure 3 that the required supporting pressure increases with the burial depth and span of a shallow tunnel. Meanwhile, the results calculated by this paper are slightly smaller than those calculated by Huang et al. [36], but the maximum difference is not more than 8%. Thus, the proposed method in this paper is validated to be effective.

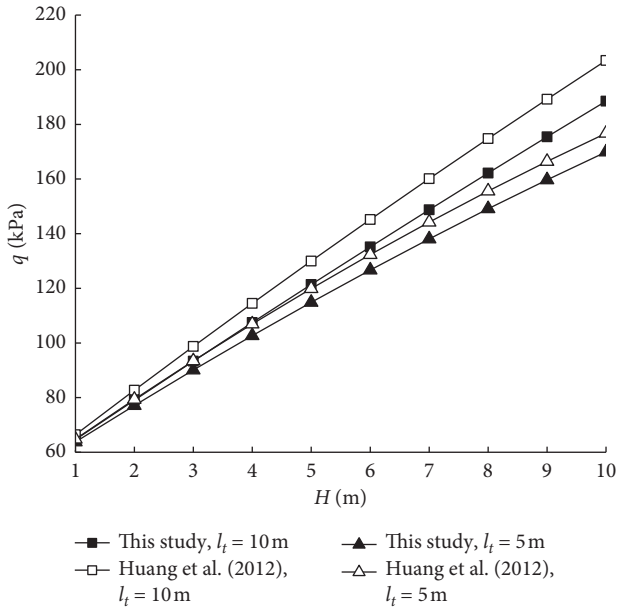

Figure 3: Comparison of the required supporting pressure with existing research works.

5.2. Comparison of the Required Supporting Pressure in 2D and 3D Mechanisms. According to the above theoretical derivation, we obtain the analytical solutions of the required supporting pressure in the 2D and 3D cases, respectively, which can provide theoretical reference for tunnel support design in practice. However, the difference between these two solutions remains elusive. To solve this problem, a shallow rectangular tunnel in two-layer rock strata is introduced as an example, and a comparative analysis is performed in this section. Figure 4 lists the required supporting pressure in the 2D and 3D mechanisms corresponding to varying tunnel burial depths, wherein the half width l_t of the tunnel is 4 m, 5 m, and 6 m, respectively. The additional ground load σ_s is 20 kPa. The strength parameters of the upper and lower rock layers are as follows: $A_1 = 0.15$, $B_1 = 0.85$, $\gamma_1 = 18\,\text{kN/m}^3$, $\sigma_{c1} = 0.5$ MPa, $\sigma_{t1} = 0.005$ MPa; $A_2 = 0.25$, $B_2 = 0.75$, $\gamma_2 = 20\,\text{kN/m}^3$, $\sigma_{c2} = 0.6$ MPa and $\sigma_{t2} = 0.006$ MPa.

It can be seen from Figure 4 that the calculation results corresponding to the 2D mechanism are greater than those corresponding to the 3D mechanism. In addition, when the tunnel burial depth is small or as the span increases, the difference between the 2D results and the 3D results decreases. This shows that the 2D failure mechanism based on the traditional plane strain hypothesis tends to overestimate the required supporting pressure and is conservative in tunnel support design. On the contrary, it is relatively economic to use the 3D failure mechanism to design the roof support. Therefore, in actual engineering, on the premise that the tunnel roof safety is guaranteed, a better support cost can be obtained with the 3D mechanism proposed in this paper. This can provide certain theoretical guidance for support design of shallow tunnels in layered strata.

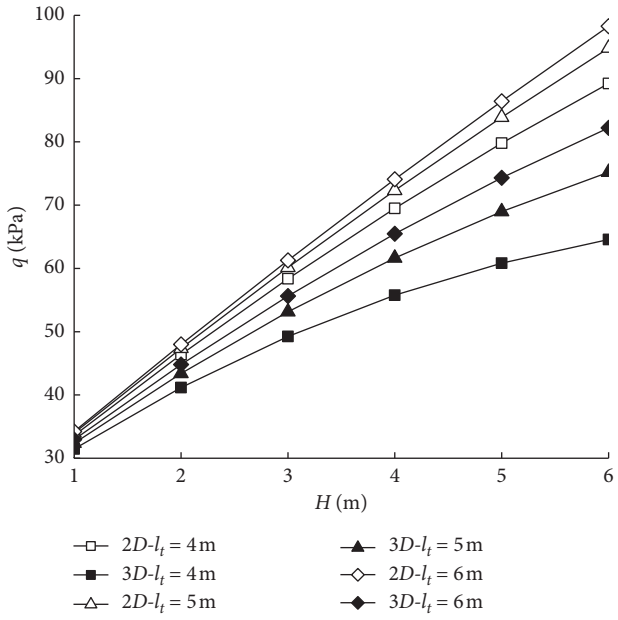

Figure 4: Comparison of the required supporting pressure in 2D and 3D mechanisms.

5.3. Comparative Analysis for a Two-Layer Tunnel Roof. In order to better guide tunnel support design, in-depth analysis on effect laws of varying parameters on the roof supporting pressure is an issue of great significance. This is because the tunnel support design can be more accurate in actual engineering only after the key factors influencing the supporting pressure are identified, thus avoiding waste of support costs and guaranteeing the safety of the support structure. In this section, the supporting pressure corresponding to the 3D failure mechanism in two roof rock layers is chosen for analysis. Figure 5 shows the change laws

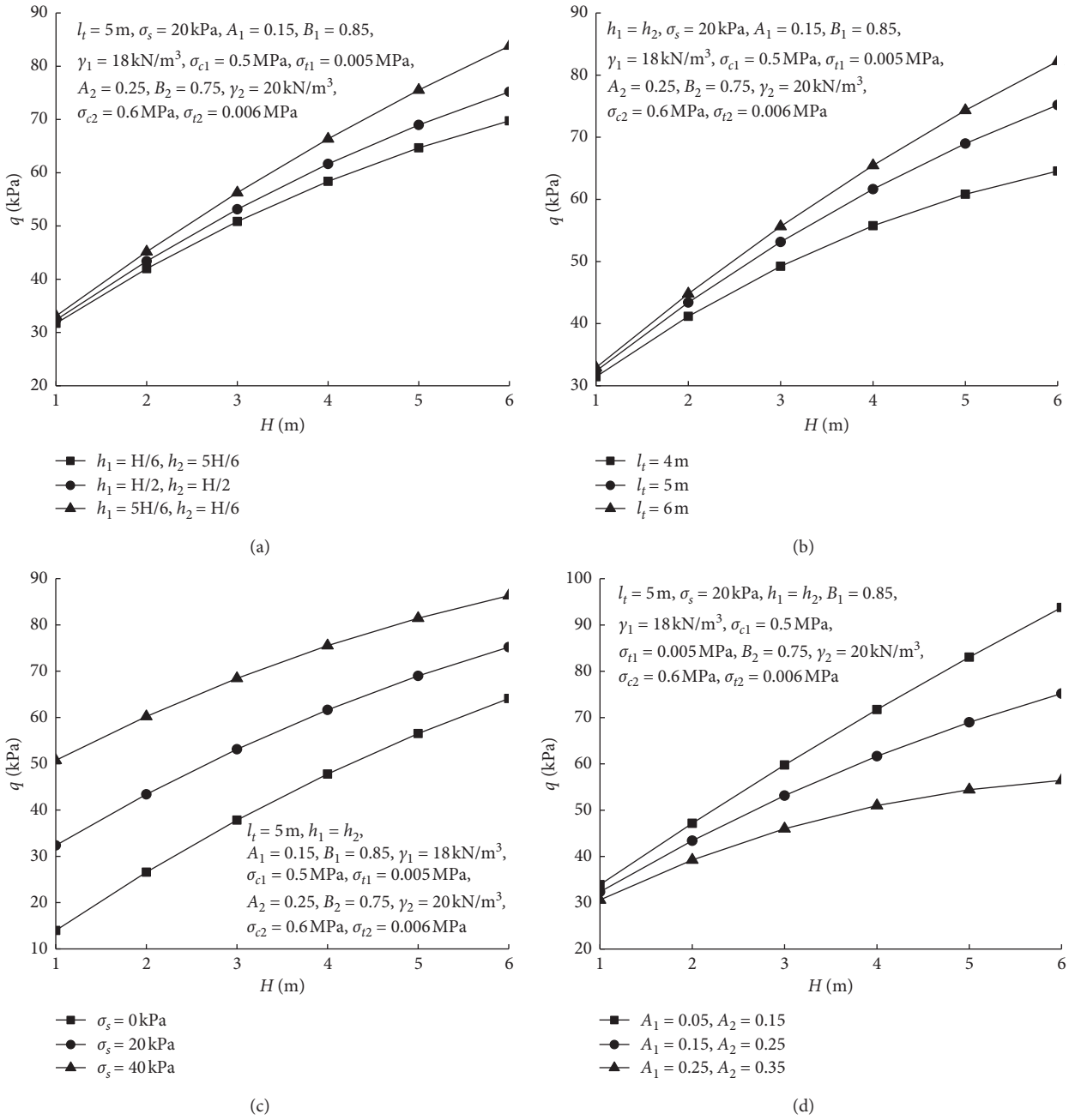

Figure 5: Continued.

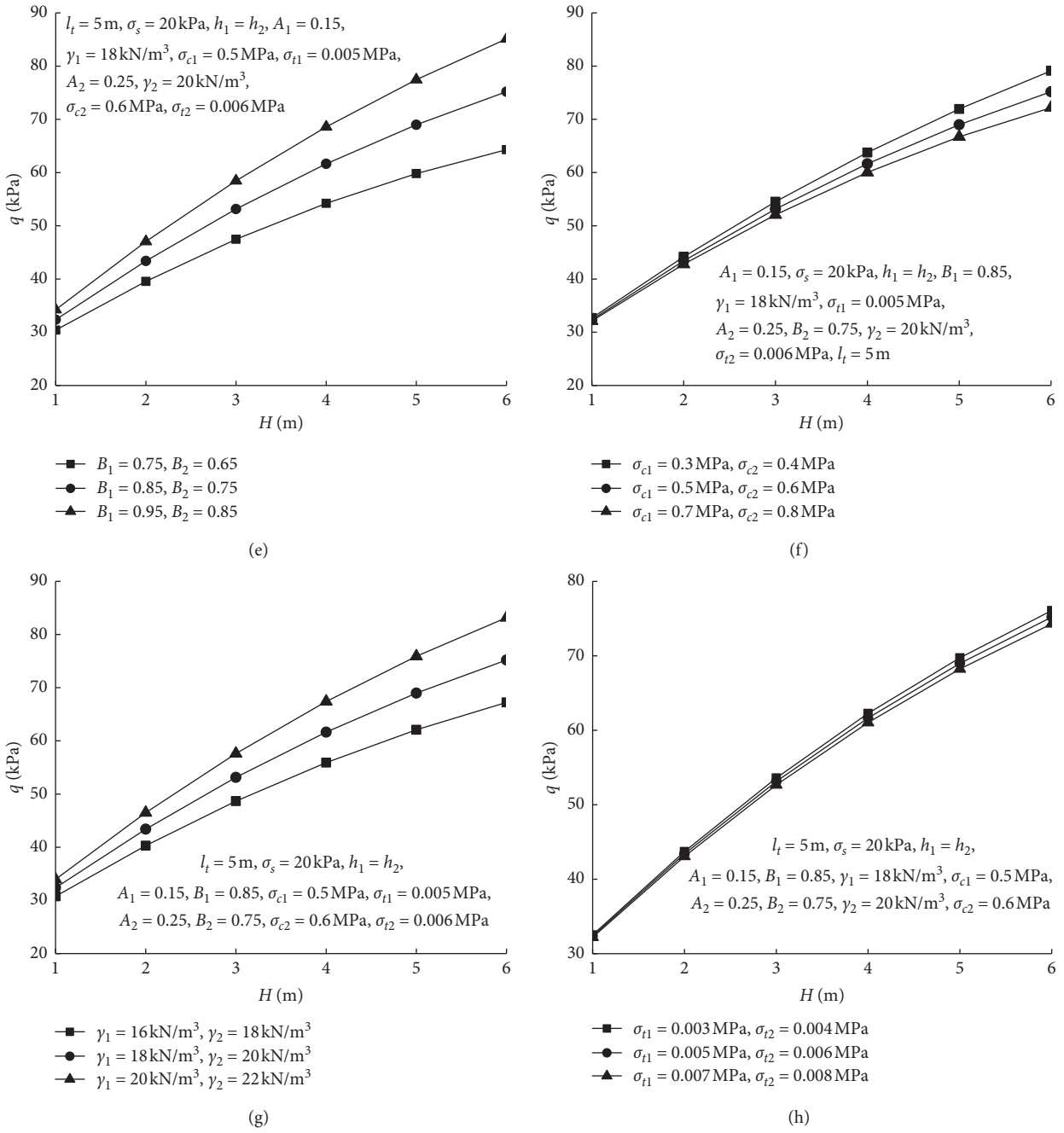

Figure 5: Change laws of the required supporting pressure under varying parameters. (a) Thickness of the upper and lower layers; (b) tunnel span; (c) additional ground load; (d) parameter A; (e) parameter B; (f) rock compressive strength; (g) rock unit weight; (h) rock tensile strength.

of the supporting pressure under varying parameters, wherein the tunnel burial depth is 1 m − 6 m; the span is 4 m − 6 m; the thickness of the upper layer is $((H/6) - (5H/6))$; the thickness of the corresponding lower layer is $((5H/6) - (H/6))$; and the additional ground load is 0 ~ 40 kPa. The strength parameters of the upper and lower layers are as follows: $A_1 = 0.05 - 0.25$, $B_1 = 0.75 - 0.95$, $\sigma_{c1} = 0.3 - 0.7$ MPa, $\sigma_{t1} = 0.003 - 0.007$ MPa, $\gamma_1 = 16 - 20$ kN/m^3; $A_2 = 0.15 - 0.35$, $B_2 = 0.65 - 0.85$, $\sigma_{c2} = 0.4 - 0.8$ MPa, $\sigma_{t2} = 0.004 - 0.008$ MPa, and $\gamma_2 = 18 - 22$ kN/m^3. Note that the other parameters are fixed when the change of a parameter is analyzed.

As can be seen in Figure 5, when the tunnel burial depth is certain, the overall strength of the roof decreases and the required supporting pressure increases as the thickness of the upper rock strata increases; this is because the strength of the lower rock layer is greater than the strength of the upper rock layer. Furthermore, the required roof supporting

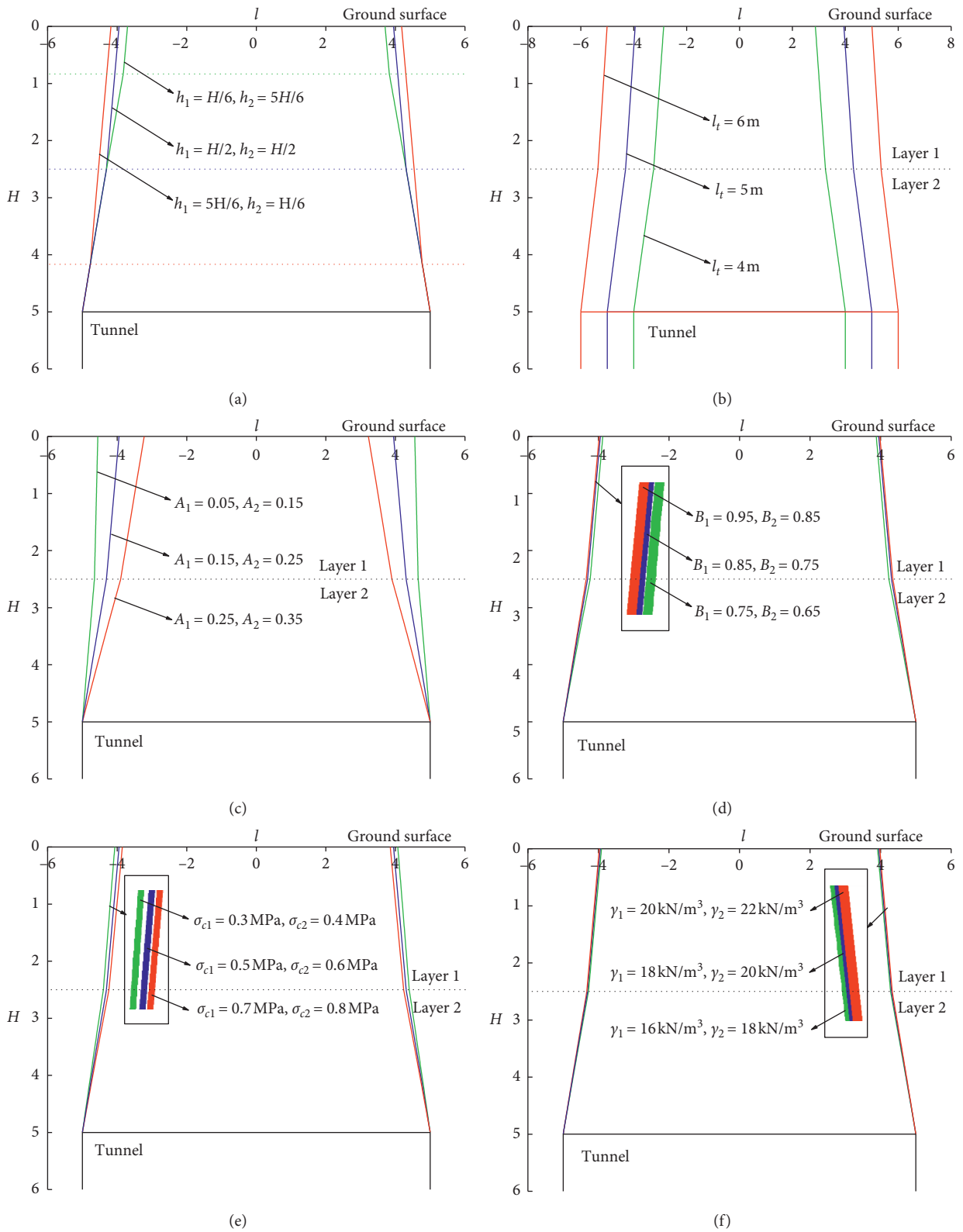

Figure 6: Change laws of the failure surface under varying parameters. (a) Thickness of the upper and lower layers; (b) tunnel span; (c) parameter A; (d) parameter B; (e) rock compressive strength; (f) rock unit weight.

pressure is positively correlated with the additional ground load, empirical parameter B, and unit weight; it is negatively correlated with empirical parameter A, compressive strength, and tensile strength of rock mass. Thus, in actual engineering, when the field geological conditions are certain, the adverse effects of the additional ground load should be

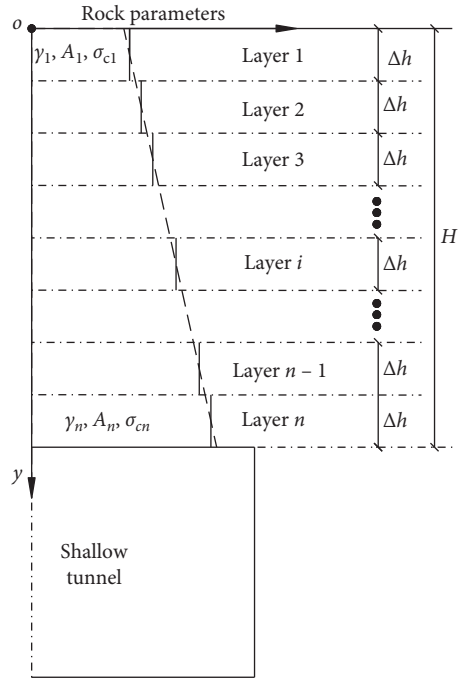

Figure 7: The nonhomogeneity of the roof rock parameters along depth.

minimized as far as possible. Meanwhile, the advance grouting technology should be adopted to improve the strength parameters of the tunnel's surrounding rock masses [39–43]. These are effective measures for reducing the required supporting pressure and support costs.

Furthermore, we plot the failure curves corresponding to the varying parameters in Figure 5, as shown in Figure 6. As can be seen in Figure 6, when the thickness of the lower layer increases, the failure range tends to decrease as the required supporting pressure decreases. As the parameter A and the compressive strength of the upper and lower layers increase, the failure range also decreases. However, as the tunnel span, parameter B, and unit weight increase, the failure range increases. In addition, the effect of parameter B, rock compressive strength, and unit weight on the failure range is less significant, while the effect of parameter A and tunnel span is more significant. Priority should be given to parameter A and tunnel span in actual engineering design.

5.4. Comparative Analysis for a Nonhomogeneous Tunnel Roof along Depth. In practical engineering, due to the influence of long-term compression from the overlying strata, the strata that the tunnel passes through may present obvious nonhomogeneous characteristics along depth. This means the rock parameters vary with depth. For example, Fraldi et al. [18] considered the profundity of the excavation and the variability of the rock mass parameters and proposed a general characterization of tunnels depth. In their research works, the unit weight γ, parameter A, and rock compressive strength σ_c are defined as the functions of the depth and tend to increase along depth. This nonhomogeneity can exert significant influence on roof collapse and safety design of tunnel support. With reference to [18], in order to incorporate this influence into the 2D and 3D layered collapse mechanisms proposed in Figure 2, we can equally divide the tunnel roof into n layers, as shown in Figure 7. Moreover, the parameters γ_1, A_1, and σ_{c1} in Layer 1 and those in Layer n are assumed to obey the following relationships:

$$\begin{cases} \gamma_n = k_\gamma \gamma_1, \\ A_n = k_A A_1, \\ \sigma_{\mathrm{cn}} = k_{\sigma_c} \sigma_{c1}, \end{cases} \tag{42}$$

where k_γ, k_A, and k_{σ_c} are nondimensional coefficients characterizing the nonhomogeneity of roof rock masses and can be obtained through laboratory test or field test. Meanwhile, for convenience, we further assume that the rock parameters in varying layers are variable and increase linearly with the depth, while the rock mass in one layer is considered locally homogeneous.

Then in Layer i, the corresponding parameters γ_i, A_i, and σ_{ci} can be expressed as

$$\begin{cases} \gamma_i = \left[1 + \dfrac{(i-1)\left(k_\gamma - 1\right)}{(n-1)}\right]\gamma_1, \\ A_i = \left[1 + \dfrac{(i-1)\left(k_A - 1\right)}{(n-1)}\right]A_1, \\ \sigma_{ci} = \left[1 + \dfrac{(i-1)\left(k_{\sigma_c} - 1\right)}{(n-1)}\right]\sigma_{c1}. \end{cases} \tag{43}$$

Furthermore, by utilizing equation (20) and equation (38), the 2D and 3D analytical solutions of the required

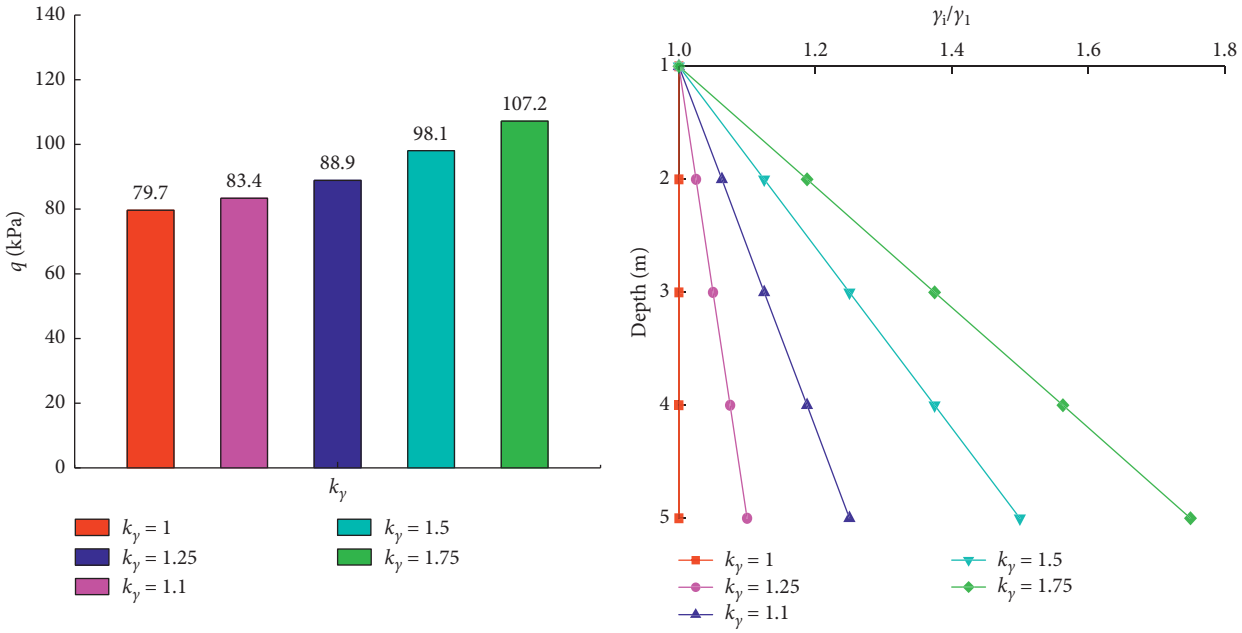

Figure 8: The required supporting pressure under varying coefficient k_γ.

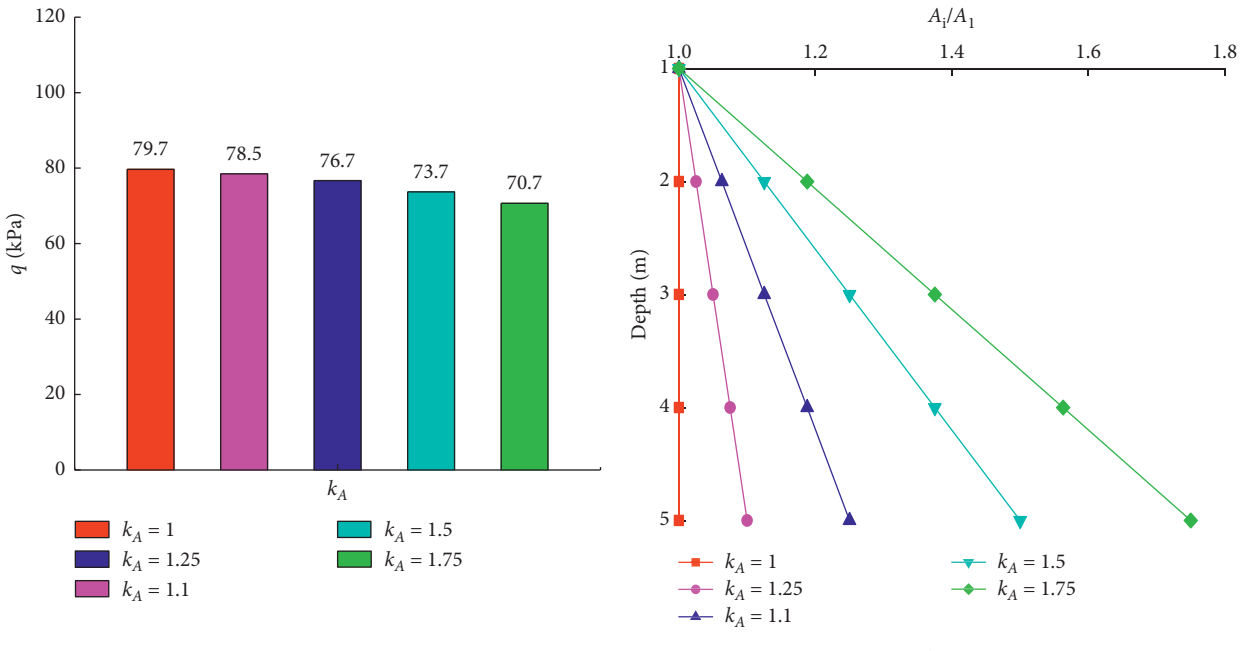

Figure 9: The required supporting pressure under varying coefficient k_A.

supporting pressure for a nonhomogeneous tunnel roof can be obtained. In order to clarify the influence of the nonhomogeneity of rock masses, the supporting pressures corresponding to varying coefficients k_γ, k_A, and k_{σ_c} under the 3D case are calculated and are listed in Figures 8–10, wherein the tunnel burial depth is 5 m, and the roof is divided into five layers. The rock parameters in Layer 1 are $A_1 = 0.15$, $B_1 = 0.85$, $\gamma_1 = 18\,\text{kN/m}^3$, $\sigma_{c1} = 0.5\,\text{MPa}$, and $\sigma_{t1} = 0.005\,\text{MPa}$. When one of the parameters varies in varying layers, the other parameters remain constant.

As can be seen in Figures 8–10, the nonhomogeneity of the rock parameters can significantly affect the required supporting pressure. When the coefficients k_γ, k_A, and k_{σ_c} are equal to 1, the rock parameters do not vary along the depth, and the tunnel roof is homogeneous. As the coefficient k_γ increases, the weight of the collapsed

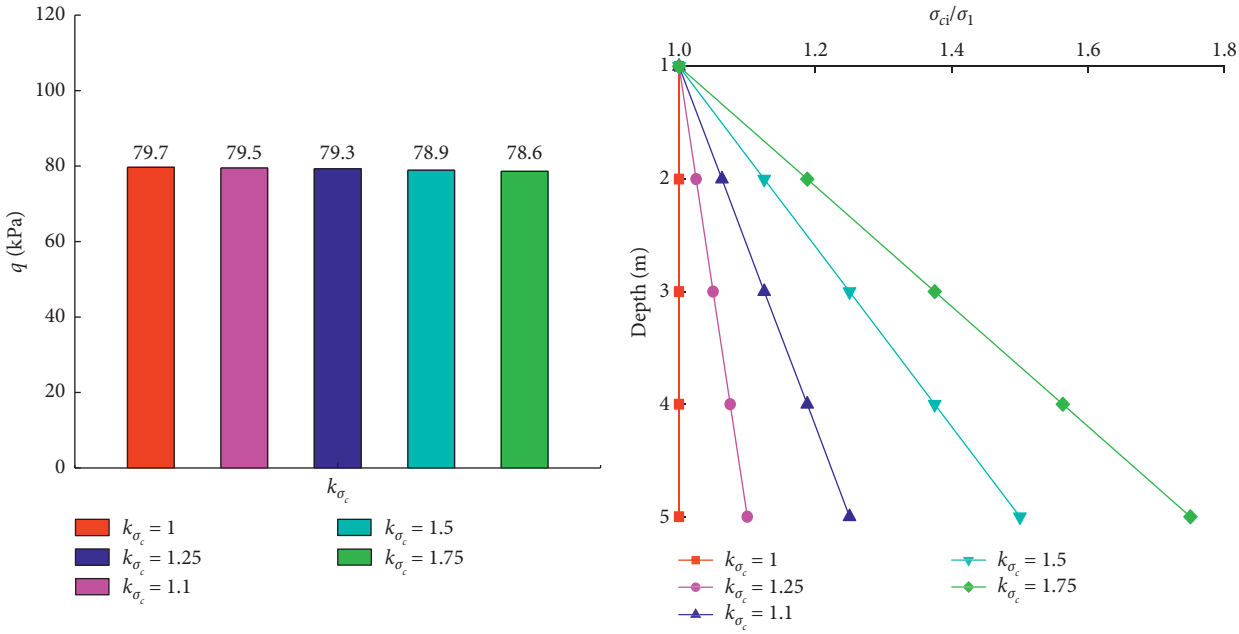

Figure 10: The required supporting pressure under varying coefficient k_{σ_c}.

rock masses increases and the required supporting pressure tends to increase accordingly. Conversely, as the coefficients k_A and k_{σ_c} increase, the whole strength of the tunnel roof increases and the required supporting pressure tends to decrease, wherein the coefficient k_γ has the most significant influence. For example, compared to $k_\gamma = 1.0$, $k_A = 1.0$, and $k_{\sigma_c} = 1.0$, the required supporting pressure corresponding to $k_\gamma = 1.75$, $k_A = 1.75$, and $k_{\sigma_c} = 1.75$ changes by 34.5%, 11.3%, and 1.38%, respectively. Thus, in tunnel support design, the nonhomogeneity of rock unit weight should be paid much care in real sceneries.

6. Conclusions

This paper constructs the 2D and 3D failure mechanisms for a shallow tunnel in layered strata. The analytical solutions of the required supporting pressure corresponding to 2D and 3D cases are derived with upper bound method. Furthermore, the effectiveness of the proposed method is validated by comparison with existing research works. The difference between the two solutions corresponding to the 2D and 3D mechanisms is clarified. The effect laws of varying parameters on the roof supporting pressure and failure range are obtained. This paper mainly draws the following conclusions:

(1) The required supporting pressure corresponding to the 2D mechanism is greater than that corresponding to the 3D mechanism. In actual engineering, on the premise that the tunnel roof safety is guaranteed, a better support cost can be obtained with the 3D failure mechanism proposed in this paper.

(2) The required supporting pressure is positively correlated with the tunnel burial depth, span, additional ground load, empirical parameter B, and unit weight; it is negatively correlated with the thickness of the rock layer with higher strength, empirical parameter A, rock compressive strength, and tensile strength. In actual engineering, the adverse effects of the additional ground load should be minimized as far as possible or the advance grouting technology should be adopted to improve the strength parameters of surrounding rock masses. These are effective measures for reducing the required supporting pressure and support costs.

(3) The tunnel failure range corresponding to the required supporting pressure is negatively correlated with the thickness of the rock layer with higher strength, parameter A, and compressive strength; it is positively correlated with the tunnel span, parameter B, and unit weight. The effect of parameter B, compressive strength, and unit weight on the failure range is less significant, while the effect of parameter A and tunnel span is more significant. Priority should be given to parameter A and tunnel span in actual engineering design.

(4) The proposed method in this paper is employed to predict the required supporting pressure for a nonhomogeneous tunnel roof along depth. The results show that the required supporting pressure is positively correlated with the nonhomogeneity coefficient of rock unit weight and is negatively correlated with the nonhomogeneity coefficients of parameter A and compressive strength.

Data Availability

The data used to support the findings of this study are included within the article.

Conflicts of Interest

The authors declare that there are no conflicts of interest regarding the publication of this paper.

Acknowledgments

The authors would like to acknowledge the financial support from the National Natural Science Foundation of China (Nos. 51704177 and 51809159), a Project of Shandong Province Higher Educational Science and Technology Program (No. J16LG04), Shandong Co-Innovation Center for Disaster Prevention and Mitigation of Civil Structures (No. XTP201911), and the Doctoral Research Fund of Shandong Jianzhu University (No. XNBS1501).

References

[1] M. Karakouzian, M. Nazari-Sharabian, and M. Karami, "Effect of overburden height on hydraulic fracturing of concrete-lined pressure tunnels excavated in intact rock: a numerical study," *Fluids*, vol. 4, no. 2, p. 112, 2019.

[2] M. Karami, A. Kabiri-Samani, M. Nazari-Sharabian, and M. Karakouzian, "Investigating the effects of transient flow in concrete-lined pressure tunnels, and developing a new analytical formula for pressure wave velocity," *Tunnelling and Underground Space Technology*, vol. 91, pp. 102–992, 2019.

[3] E. Leca and L. Dormieux, "Upper and lower bound solutions for the face stability of shallow circular tunnels in frictional material," *Géotechnique*, vol. 40, no. 4, pp. 581–606, 1990.

[4] I.-M. Lee and S.-W. Nam, "The study of seepage forces acting on the tunnel lining and tunnel face in shallow tunnels," *Tunnelling and Underground Space Technology*, vol. 16, no. 1, pp. 31–40, 2001.

[5] K. Yamamoto, A. V. Lyamin, D. W. Wilson, S. W. Sloan, and A. J. Abbo, "Stability of a single tunnel in cohesive-frictional soil subjected to surcharge loading," *Canadian Geotechnical Journal*, vol. 48, no. 12, pp. 1841–1854, 2011.

[6] G. Mollon, D. Dias, and A.-H. Soubra, "Continuous velocity fields for collapse and blowout of a pressurized tunnel face in purely cohesive soil," *International Journal for Numerical and Analytical Methods in Geomechanics*, vol. 37, no. 13, pp. 2061–2083, 2013.

[7] M. Huang and C. Song, "Upper-bound stability analysis of a plane strain heading in non-homogeneous clay," *Tunnelling and Underground Space Technology*, vol. 38, pp. 213–223, 2013.

[8] C. Zhang, K. Han, and D. Zhang, "Face stability analysis of shallow circular tunnels in cohesive-frictional soils," *Tunnelling and Underground Space Technology*, vol. 50, pp. 345–357, 2015.

[9] K. Han, C. Zhang, W. Li, and C. Guo, "Face stability analysis of shield tunnels in homogeneous soil overlaid by multilayered cohesive-frictional soils," *Mathematical Problems in Engineering*, vol. 2016, Article ID 1378274, 9 pages, 2016.

[10] W. Li, C. Zhang, W. Zhu, and D. Zhang, "Upper-bound solutions for the face stability of a non-circular NATM tunnel in clays with a linearly increasing undrained shear strength with depth," *Computers and Geotechnics*, vol. 114, pp. 103–136, 2019.

[11] W. Li and C. P. Zhang, "Face stability analysis for a shield tunnel in anisotropic sands," *International Journal of Geomechanics*, vol. 20, no. 5, 2019.

[12] E. Hoek and E. T. Brown, *Underground Excavations in Rock*, CRC Press, Boca Raton, FL, USA, 1980.

[13] E. Hoek and E. T. Brown, "Practical estimates of rock mass strength," *International Journal of Rock Mechanics and Mining Sciences*, vol. 34, no. 8, pp. 1165–1186, 1997.

[14] R. Baker, "Nonlinear mohr envelopes based on triaxial data," *Journal of Geotechnical and Geoenvironmental Engineering*, vol. 130, no. 5, pp. 498–506, 2004.

[15] M. Singh, A. Raj, and B. Singh, "Modified mohr-coulomb criterion for non-linear triaxial and polyaxial strength of intact rocks," *International Journal of Rock Mechanics and Mining Sciences*, vol. 48, no. 4, pp. 546–555, 2011.

[16] M. Fraldi and F. Guarracino, "Limit analysis of collapse mechanisms in cavities and tunnels according to the hoek-brown failure criterion," *International Journal of Rock Mechanics and Mining Sciences*, vol. 46, no. 4, pp. 665–673, 2009.

[17] M. Fraldi and F. Guarracino, "Analytical solutions for collapse mechanisms in tunnels with arbitrary cross sections," *International Journal of Solids and Structures*, vol. 47, no. 2, pp. 216–223, 2010.

[18] M. Fraldi, R. Cavuoto, A. Cutolo, and F. Guarracino, "Stability of tunnels according to depth and variability of rock mass parameters," *International Journal of Rock Mechanics and Mining Sciences*, vol. 119, pp. 222–229, 2019.

[19] F. Huang and X. L. Yang, "Upper bound limit analysis of collapse shape for circular tunnel subjected to pore pressure based on the hoek-brown failure criterion," *Tunnelling and Underground Space Technology*, vol. 26, no. 5, pp. 614–618, 2011.

[20] C.-p. Zhang, K.-h. Han, Q. Fang, and D.-l. Zhang, "Functional catastrophe analysis of collapse mechanisms for deep tunnels based on the hoek-brown failure criterion," *Journal of Zhejiang University Science A*, vol. 15, no. 9, pp. 723–731, 2014.

[21] X. L. Yang and F. Huang, "Three-dimensional failure mechanism of a rectangular cavity in a hoek-brown rock medium," *International Journal of Rock Mechanics and Mining Sciences*, vol. 61, pp. 189–195, 2013.

[22] F. Huang, X. L. Yang, and T. H. Ling, "Prediction of collapsing region above deep spherical cavity roof under axis-symmetrical conditions," *Rock Mechanics and Rock Engineering*, vol. 47, no. 4, pp. 1511–1516, 2014.

[23] K. Guan, W. C. Zhu, L. L. Niu, and Q. Y. Wang, "Three-dimensional upper bound limit analysis of supported cavity roof with arbitrary profile in Hoek-Brown rock mass," *Tunnelling and Underground Space Technology*, vol. 69, pp. 147–154, 2017.

[24] C. B. Qin, X. L. Yang, Q. J. Pan, Z. B. Sun, L. L. Wang, and T. Miao, "Upper bound analysis of progressive failure mechanism of tunnel roofs in partly weathered stratified hoek-brown rock masses," *International Journal of Rock Mechanics and Mining Sciences*, vol. 74, pp. 157–162, 2015.

[25] X. L. Yang and C. Yao, "Stability of tunnel roof in nonhomogeneous soils," *International Journal of Geomechanics*, vol. 18, no. 3, Article ID 06018002, 2018.

[26] X. L. Yang, T. Zhou, and W. T. Li, "Reliability analysis of tunnel roof in layered hoek-brown rock masses," *Computers and Geotechnics*, vol. 104, pp. 302–309, 2018.

[27] X. L. Yang and C. Yao, "Axisymmetric failure mechanism of a deep cavity in layered soils subjected to pore pressure," *International Journal of Geomechanics*, vol. 17, no. 8, Article ID 04017031, 2017.

[28] C. Qin and S. C. Chian, "2D and 3D stability analysis of tunnel roof collapse in stratified rock: a kinematic approach," *International Journal of Rock Mechanics and Mining Sciences*, vol. 100, pp. 269–277, 2017.

[29] C. B. Qin, S. C. Chian, and X. L. Yang, "3D limit analysis of progressive collapse in partly weathered hoek–brown rock banks," *International Journal of Geomechanics*, vol. 17, no. 7, Article ID 04017011, 2017.

[30] C. Qin and S. C. Chian, "Revisiting crown stability of tunnels deeply buried in non-uniform rock surrounds," *Tunnelling and Underground Space Technology*, vol. 73, pp. 154–161, 2018.

[31] X. L. Yang and F. Huang, "Collapse mechanism of shallow tunnel based on nonlinear hoek-brown failure criterion," *Tunnelling and Underground Space Technology*, vol. 26, no. 6, pp. 686–691, 2011.

[32] X. L. Yang and K. F. Li, "Roof collapse of shallow tunnel in layered hoek-brown rock media," *Geomechanics and Engineering*, vol. 11, no. 6, pp. 867–877, 2016.

[33] H. T. Wang, L. G. Wang, S. C. Li, Q. Wang, P. Liu, and X. J. Li, "Roof collapse mechanisms for a shallow tunnel in two-layer rock strata incorporating the influence of groundwater," *Engineering Failure Analysis*, vol. 98, pp. 215–227, 2019.

[34] H. T. Wang, P. Liu, C. Liu, X. Zhang, Y. Yang, and L. Y. Liu, "Three-dimensional upper bound limit analysis on the collapse of shallow soil tunnels considering roof stratification and pore water pressure," *Mathematical Problems in Engineering*, vol. 2019, Article ID 8164702, 15 pages, 2019.

[35] C. Lyu and Z. Zeng, "Upper bound limit analysis of unsymmetrical progressive collapse of shallow tunnels in inclined rock stratum," *Computers and Geotechnics*, vol. 116, p. 103199, 2019.

[36] F. Huang, X.-l. Yang, and L.-h. Zhao, "Upper bound solution of supporting pressure for a shallow square tunnel based on the hoek-brown failure criterion," *Journal of Zhejiang University Science A*, vol. 13, no. 4, pp. 284–292, 2012.

[37] B. Jiang, Q. Wang, S. C. Li et al., "The research of design method for anchor cables applied to cavern roof in water-rich strata based on upper-bound theory," *Tunnelling and Underground Space Technology*, vol. 53, pp. 120–127, 2016.

[38] W. F. Chen, *Limit Analysis and Soil Plasticity*, Elsevier scientific publishing company, Amsterdam, Netherlands, 1975.

[39] R. Liu, N. Huang, Y. Jiang, H. Jing, and L. Yu, "A numerical study of shear-induced evolutions of geometric and hydraulic properties of self-affine rough-walled rock fractures," *International Journal of Rock Mechanics and Mining Sciences*, vol. 127, p. 104211, 2020.

[40] R. Liu, M. He, N. Huang, Y. Jiang, and L. Yu, "Three-dimensional double-rough-walled modeling of fluid flow through self-affine shear fractures," *Journal of Rock Mechanics and Geotechnical Engineering*, vol. 12, no. 1, pp. 41–49, 2020.

[41] Q. Wang, H. Gao, H. Yu, B. Jiang, and B. Liu, "Method for measuring rock mass characteristics and evaluating the grouting-reinforced effect based on digital drilling," *Rock Mechanics and Rock Engineering*, vol. 52, no. 3, pp. 841–851, 2019.

[42] H. T. Wang, S. C. Li, Q. Wang et al., "Investigating the supporting effect of rock bolts in varying anchoring methods in a tunnel," *Geomechanics and Engineering*, vol. 19, no. 6, pp. 485–498, 2019.

[43] W. T. Li, N. Yang, Y. C. Mei, Y. H. Zhang, L. Wang, and H. Y. Ma, "Experimental investigation of the compression-bending property of the casing joints in a concrete filled steel tubular supporting arch for tunnel engineering," *Tunnelling and Underground Space Technology*, vol. 96, 2020.